

Failure model calibration of a DP1000 dual phase steel using solid and shell elements for crash simulation

Florence Andrieux, Silke Klitschke, Andreas Trondl

Fraunhofer Institute for Mechanics of Materials IWM

1 Introduction

With the trend towards lightweight construction, advanced high-strength steel (AHSS) is increasingly being used in automotive structural components. Since the ductility of high strength steels is relatively low, damage behaviour of these materials must be accurately modelled. In automotive structures AHSS components are usually discretized with shell elements. With the increase of computation capacity attempts with solid elements are made to capture the loading state more accurately, especially after necking. For this reason, it is convenient to develop a method which enables a systematic model calibration from the 3D to the 2D loading situation. The failure strain of metallic materials depends on stress state. In the past years several studies have shown that the stress triaxiality is not sufficient to describe failure and empirical models were extended to consider the effect of Lode parameter. Recently it was also shown that the amount of bending seems to influence failure, namely i.e. the failure strain increases with the amount of bending.

In this work a DP1000 dual phase steel has been investigated both experimentally and numerically. To study the dependence of damage behaviour on loading state, smooth tensile-, notched, shear, bending, punch and Nakajima tests were performed. A general damage model based on a critical failure strain depending on triaxiality and Lode parameter was calibrated for solid elements. The failure strain curve for shell elements was derived from the failure surface for solid elements considering the relationship between triaxiality and Lode parameter under plane stress condition. Moreover, the influence of the bending factor was introduced into the failure model for shell elements. FE simulations with LS-Dyna were performed to determine the local values of triaxiality, Lode parameter and bending ratio for each specimen type. The applied damage models were calibrated and verified by simulating all specimen tests.

2 Experimental investigation

To investigate the failure behaviour of the DP1000 dual phase steel HCT980X+Z100MB six specimen geometry types were extracted (water jet cutting) from a sheet of 1.5 mm thickness to generate a large range of stress states. Tensile tests on smooth, notched and shear specimens as well as bending, punch and Nakajima tests were performed. The three tensile tests induce uniaxial, plane strain and shear (zero triaxiality) loading under pure membrane state, i.e., with stress or strain uniformly distributed through the thickness. To investigate the influence of bending, a plane-strain bending tests in accordance with the German guideline [1] were carried out for which a plate lying on two supports closed together is bended by a very sharp punch. A plane strain loading under bending is obtained. The punch and Nakajima tests both generate equibiaxial tension. The difference is the specimen size; in the Nakajima test the die has a diameter of 105 mm for a punch diameter of 100 mm, in the punch test the diameter of the die is of 27 mm and this of the punch is of 20 mm. As a result, a quasi-membrane stress state is obtained with the Nakajima test while some bending is present in the punch test. Another difference between these test types is that more material is tested in the Nakajima test than in the punch test. Tests were performed under quasi-static loading and force displacement curves were registered. Local strains were determined by digital image correlation (DIC). The results are shown in Fig.2, 3 and 5.

3 Model for solid elements

The simulations were performed with the LS-Dyna version R12. Fully integrated solid elements (ELFORM 2) were used with an element length of 0.3 mm in the regions of interest. As a result, the 1.5 mm thickness is discretized with 5 elements.

3.1 Deformation model

The von Mises model was applied using the material type `*MAT_PIECEWISE_LINEAR_PLASTICITY`. The yield stress was defined based on the tensile results using inverse simulations.

3.2 Failure model

A strain-based failure model was used in combination with the deformation model through the option `*MAT_ADD_DAMAGE_GISSMO`. In GISSMO (Generalized Incremental Stress-State dependent damage MOdel). The cumulative damage is driven by the plastic strain weighted by the failure strain. A quadratic damage evolution is used (the parameter DMGEXP is set to 2). The element is deleted when the damage reaches the critical value of 1. In this work no coupling between damage and stress is considered; the damage is solely used as failure criteria. The failure strain is supposed to depend on stress triaxiality and Lode parameter. The model proposed by Bai and Wierzbicki in [2] was retained. The fracture locus is based on 3 boundary limits by Lode parameters equal to -1, 0 and 1. The failure strain for each three Lode parameters is chosen according to the Rice and Tracey model [3] of void growth leading to the exponential function of stress triaxiality (1):

$$\varepsilon_f^l(\eta) = C_1^l \exp(-C_2^l \eta), \quad l = -, 0, + \quad (1)$$

In (1) η is the stress triaxiality and the superscript l taking the symbols -, 0 or + indicates respectively a Lode parameter of -1, 0 or 1. ε_f is the failure strain and C_1 and C_2 are two material parameters, each for Lode parameters of -1, 0 and 1. Regarding the effect of Lode parameter a parabolic function is proposed to interpolate between the three boundary failure strains defined by (1) The failure strain is finally expressed by (2) where ξ denotes the Lode parameter.

$$\varepsilon_f(\eta, \xi) = \left[\frac{1}{2}(\varepsilon_f^+ + \varepsilon_f^-) - \varepsilon_f^0 \right] \xi^2 + \frac{1}{2}(\varepsilon_f^+ - \varepsilon_f^-) \xi + \varepsilon_f^0 \quad (2)$$

The six failure parameters were fitted at the experimental load-displacement curves. The bending and punch tests were excluded from the parameter calibration. These tests have almost the same triaxiality and Lode parameter values as the notch and Nakajima test respectively, but they show different failure strains (see Fig.1). For the calibration only the tests under membrane loading were considered, not those having a bending component.

The calibrated failure surface is shown on Fig. 1.a with the experimental failure points. They are obtained numerically in the critical element at the failure time determined from the experimental load-displacement curves. Fig1.b gives the failure strain vs. triaxiality for the three bounding cases and for plane stress condition together with the loading paths in colour from tensile (T), notched (N), shear (S), bending (B), Nakajima (Naka), and punch (P) tests. The full symbols denote experimental failure points. The open symbols represent the values obtained with DIC method for the last state bevor crack initiation. The triaxiality is estimated from the principal strain using the plane stress assumption. Fig1.c describes the failure strain vs. Lode parameters with the experimental loading paths. From Figures 1.b and 1.c the tests can be roughly sorted into three classes covering the 3 bounding cases:

1. $\xi \approx 1$: tensile test
2. $\xi \approx 0$: shear, notch, and bending tests
3. $\xi \approx -1$: punch and Nakajima tests

It is worth noting that the punch and Nakajima tests show the same triaxiality and Lode parameter but the failure strain for punch is higher than for Nakajima test. In the same manner the notch and bending tests have similar triaxiality and Lode parameter but also different failure strains. This effect cannot be described using a failure curve depending on triaxiality and Lode parameter.

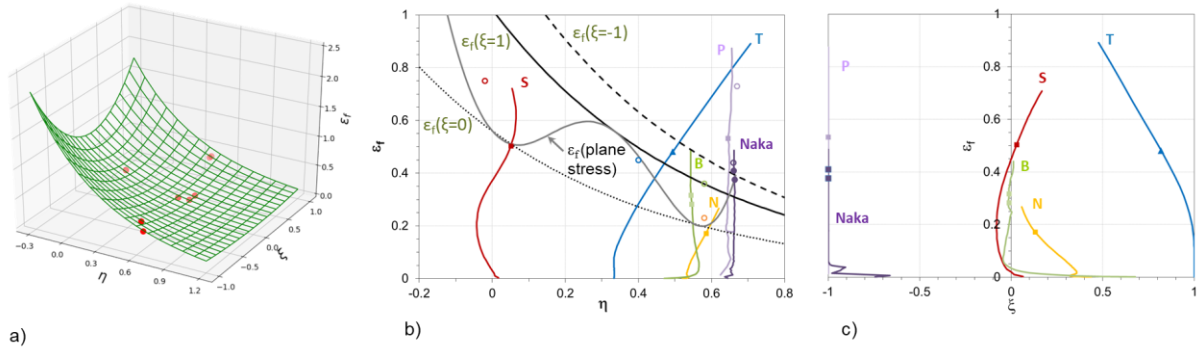


Fig. 1: a) Failure surface with experimental points. b) Failure strain vs. triaxiality for the three bounding cases and for plane stress condition together with the loading paths in colour. c) Failure strain vs. Lode parameter together with the loading paths in colour. Symbols for failure determined numerically (full) and from DIC (open). Tensile (T), notched (N), shear (S), bending (B), Nakajima (Naka), and punch (P).

4 Model for shell elements

Fully integrated shell elements (ELFORM 16) were used also with an element length of 0.3 mm in the regions of interest and five integration points over the thickness.

4.1 Deformation model

The von Mises model was also retained for the simulation with shell elements and the yield stress used for solid elements was directly applied.

4.2 Failure model

The effect of bending factor on failure strain was first investigated in the forming community and several works show that the FLD curves are influenced by the amount of bending, see for instance [4]. For crash application the same influence of bending factor was also observed, and it was shown that the failure strain seems to increase with increasing bending amount, see for example [5] and [6]. In the recent versions of LS-Dyna it is possible to define a failure curve depending on triaxiality and bending indicator in the GISSMO failure model. This feature is only available for shell elements, the bending indicator Ω is defined by equation (3):

$$\Omega = \frac{1}{2} \frac{|\varepsilon_{p,33}^T - \varepsilon_{p,33}^B|}{\max(|\varepsilon_{p,33}^T|, |\varepsilon_{p,33}^B|)} \quad (3)$$

In (3) $\varepsilon_{p,33}$ indicates the plastic strain in thickness direction, the superscripts T and B indicate the upper (top) and lower (bottom) integration point respectively. The bending indicator is then equal to 0 for pure membrane loading and 1 for pure bending. That way the bending indicator is a global indicator of the loading at the element level, not at integration point level as for damage. The failure surface from solid elements was also retained to derive the failure curve for membrane loading ($\varepsilon_f(\eta, \Omega=0)$), considering the relationship between triaxiality and Lode parameter under plane stress condition (see Fig. 1.b). The failure strain for bending loading ($\varepsilon_f(\eta, \Omega=1)$) was obtained by scaling the membrane failure curve as defined by (4). The scaling factor of 2.5 was determined using the bending test.

$$\varepsilon_f(\eta, \Omega=1) = 2.5 \varepsilon_f(\eta, \Omega=0) \quad (4)$$

5 Simulation results

The simulations of all specimen tests were performed using solid and shell elements. The force displacement curves are given in Figures 2, 3 and 5. The curves in colour show the experimental results, the curves in black or grey the simulations. The punch, Nakajima, and bending test simulations with shell elements were performed using both a failure curve depending solely on triaxiality and a failure surface depending on triaxiality and bending indicator. For tensile, notch and shear tests there is no influence of bending indicator with remains zero, only one curve is given. The dashed lines represent the results obtained with solid elements, the solid ones with shell elements. The grey solid lines indicate

the results with a failure curve depending on triaxiality, the black ones with a failure surface depending on triaxiality and bending indicator.

For the smooth, notched and shear tensile tests the simulations agree well with the experiments., in the simulations with shell elements the failure is slightly underestimated since the failure strain calibrated for solid elements were directly used for shell without adjustment although the stress state can deviate due to the plane stress assumption which is not always fulfilled, especially near failure when necking occurs. The deviations remain acceptable.

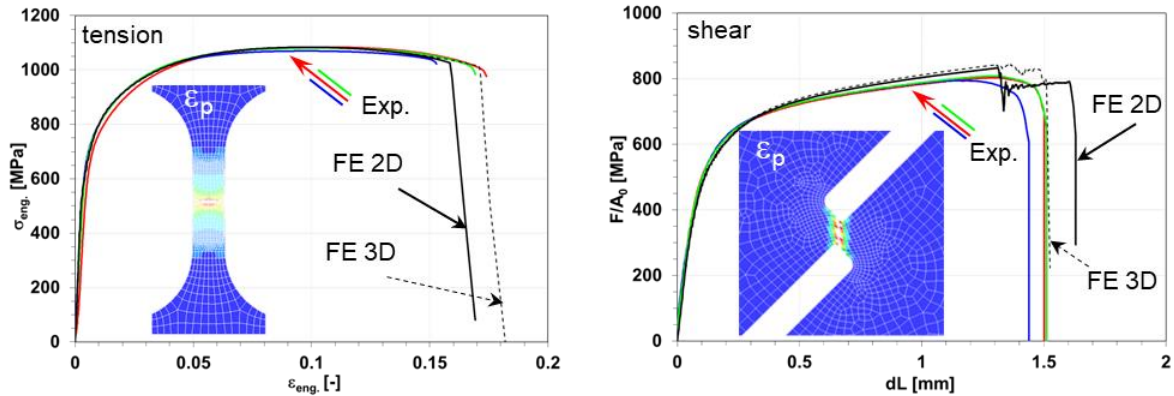


Fig.2: Experimental and calculated nominal stress vs. nominal strain or elongation curves with the plastic strain distribution at failure initiation for tensile (left) and shear (right) test.

The simulation of bending test with solid elements underestimates the bending angle at failure (Fig.3 left). This is due to the fact that for failure calibration the notch test was retained, with the failure model used in this work it is not possible to describe both tests simultaneously. This is illustrated by Fig.4.a and b showing the time evolution of the plastic strain and the triaxiality for the 5 elements in a row under the punch. The element directly under the punch has the identity 1, the element on the opposite outer surface the identity 5. The crack initiation is indicated by a vertical line. Fig.4.b demonstrates that a plane-strain bending condition is achieved, the outer elements being under tensile plane-strain ($\eta \approx 1/\sqrt{3}$), the inner elements under compressive plane-strain ($\eta \approx -1/\sqrt{3}$). On Fig.4.b the critical strain determined from the notch test used for the calibration of the failure surface is indicated, it explains the too early prediction of failure in the bending test. When a crack initiates, the 2 elements on the outer side of the specimen (elements 4 and 5) have reached the critical strain obtained under membrane condition. This could be an explanation why the amount of bending affects failure; the critical strain needs to be attained not locally but in a larger volume, in this case the thickness. This result is in contradiction with the assumption of Costas et al. [5], who argue that the failure strain adopted for a mesh of fine solid elements can be considered as an intrinsic material property and can also determine when failure initiates under pure bending.

Using shell elements with the same failure model, the results are comparable. Adopting the model with influence of the bending indicator, the failure can be exactly predicted. In the bending test, the specimen cracks only superficially, the side in compression, below the punch, does not break in the experiment as it does in simulation, as shown by Fig.4.c.

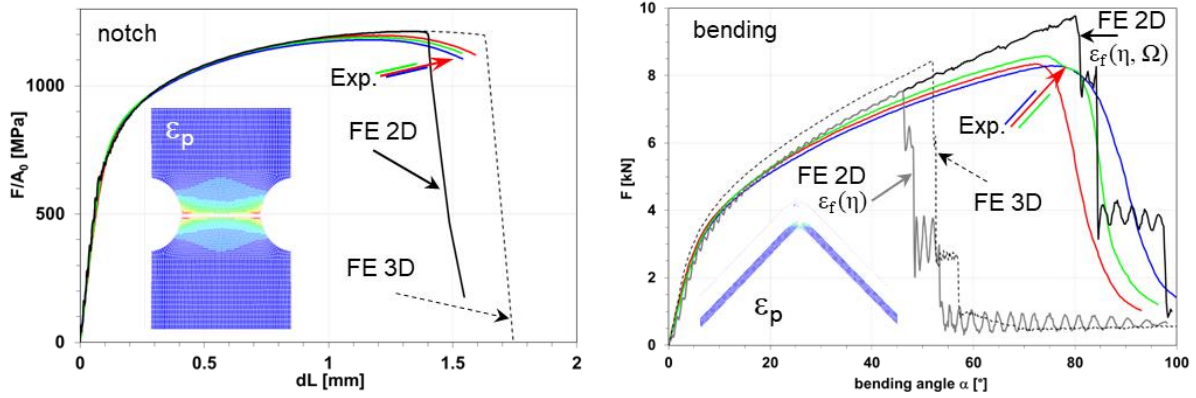


Fig.3: Experimental and calculated nominal stress vs. elongation curves for notch test (left) and force vs. angle curves for bending test (right) with the plastic strain distribution at failure initiation.

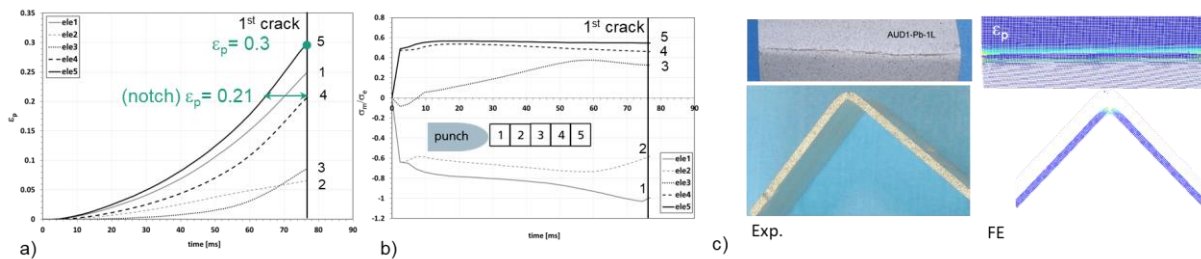


Fig.4: Plastic strain a) and triaxiality b) time evolution for the 5 elements in a row under the punch in the bending test. c) Bending specimen after test in experiment (left) and simulation (right).

The simulation of the Nakajima test with solid elements agrees very well with the experiment for the deformation and failure behaviour (Fig.5 left). With shell elements using the same failure model the final rupture is slightly underestimated. This is corrected using the failure model with influence of bending. The difference between the simulations with and without consideration of the bending effect is minor because the loading is near to a membrane state. The failure is significantly underestimated in the simulation of the punch test with solid elements (Fig.5 right). The simulation with shell elements underestimates the failure displacement even more without consideration of bending effect. With the approach with bending effect the failure is only slightly underestimated, and the prediction of the punch test is acceptable.

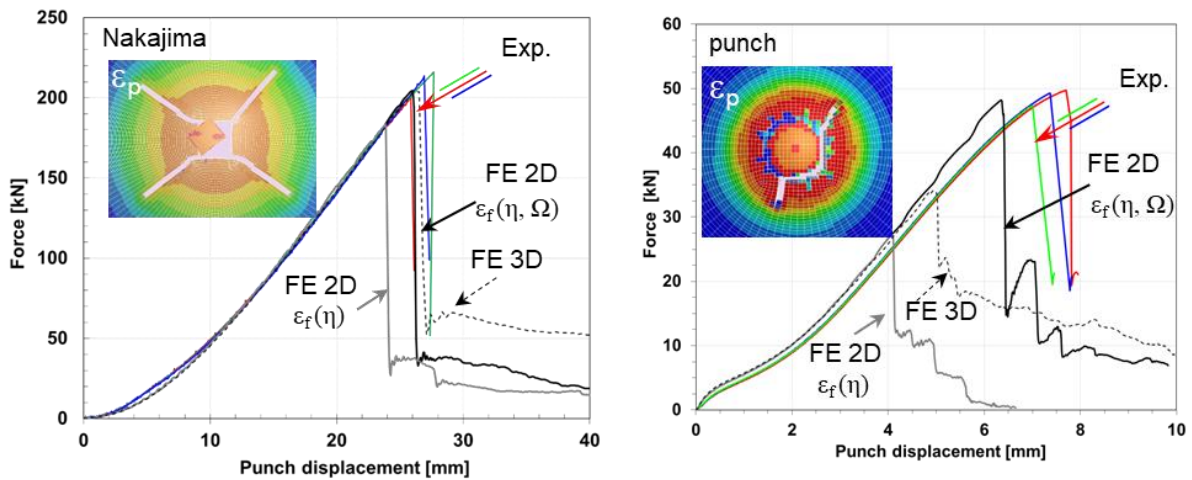


Fig.5: Experimental and calculated force vs. displacement curves for Nakajima (left) and punch test (right) with the plastic strain distribution at failure.

The reason is that for the failure calibration the Nakajima test was retained and both tests show almost the same triaxiality and Lode parameter which are very close to the theoretical values of 2/3 and -1 characterizing the equibiaxial tension (see Fig.1). However, the local strain at failure initiation is much higher in the punch test than in the Nakajima test (light and deep purple symbols in Fig1.b). The different local strains near failure in Nakajima (left) and punch tests (right) are also illustrated in Fig.6 comparing the equivalent strain distributions obtained by DIC method (ARAMIS) just before failure for Nakajima (left) and punch specimen (right).

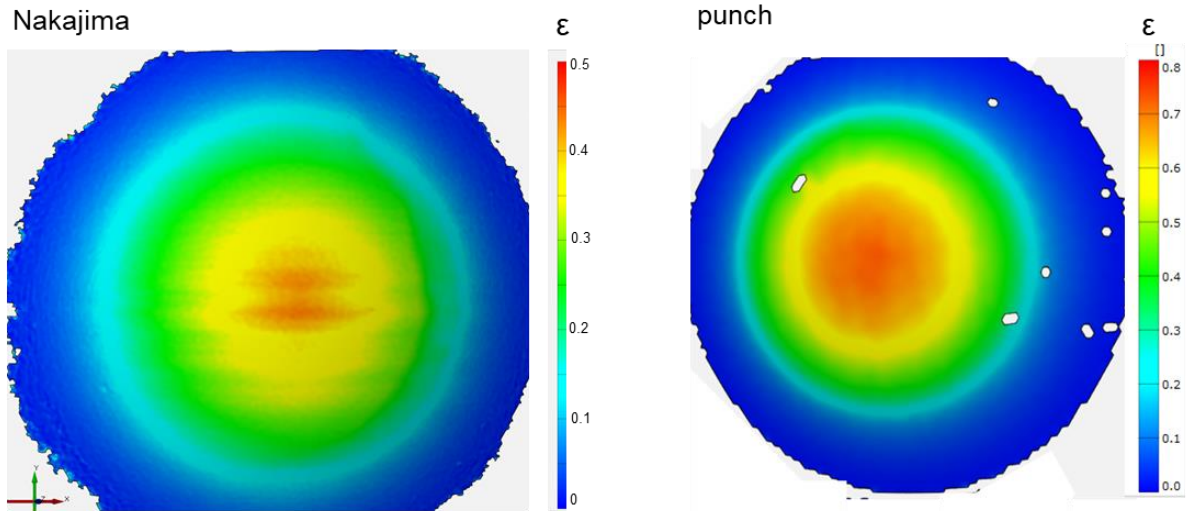


Fig.6: ARAMIS equivalent strain distribution for Nakajima (left) and punch specimen (right) just before failure.

The simulation of the punch test with solid elements underestimates the displacement at failure, because for failure calibration the Nakajima test was retained. Fig.7. shows that for the punch test a bending amount is present however the gradients through the thickness remain moderate. On Fig.7.b the critical strain determined from the Nakajima test is indicated. This explains the early failure prediction in the punch test. However, in this case the specimen reaches the critical strain determined from the Nakajima test through the entire thickness befor it fails. The explanation suggested above to explain the different failure strains between the notch and the bending specimen is no longer valid or not the only effect to be considered.

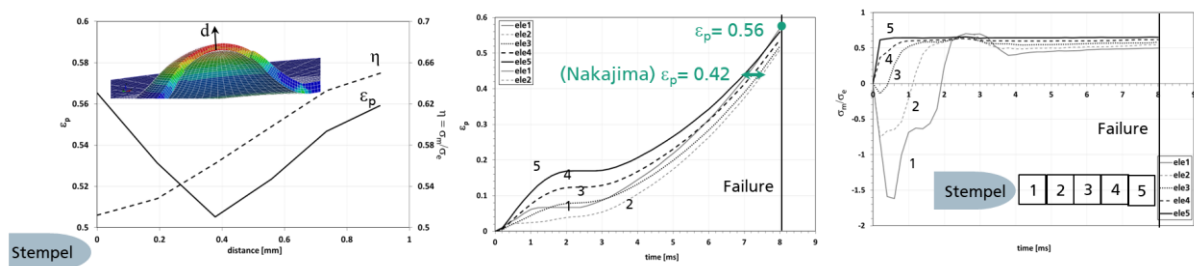


Fig.7: a) Plastic strain and triaxiality evolution over thickness just befor failure, plastic strain b) and triaxiality c) time evolution for the 5 elements in the raw under the punch.

6 Summary

In this work failure models for solid and shell elements were investigated. A Bai-Wierzbicki model, with a failure strain depending on stress triaxiality and Lode parameter, was retained for solid element. With this model it was possible to well describe the failure for all tests in or near a membrane state (tensile, notch, shear and Nakajima). The failure was underestimated for all tests with a bending component (bending and punch). It was pointed out that the experimental set only covered the three boundary limits given by Lode parameters equal to -1, 0 and 1, it was not possible to achieve a large variation of the Lode parameter. For shell elements it was possible to successfully apply the same failure model,

considering only the relationship between triaxiality and Lode parameter under plane stress condition. The same deficit as for solid elements was obtained for all test having a bending amount, namely the failure displacement was largely underestimated. A model with influence of the bending indicator was calibrated and this discrepancy was eliminated. It is shown that the predictions were more accurate using shell elements because of the possibility to account for the bending ratio influence, what is not possible using solid elements. The influence of bending on failure needs to be further investigated.

7 Acknowledgement

The research project IFG 21713 N/ P1518 "Systematic calibration, validation and evaluation of failure models for crash simulation of advanced high strength steel sheets (AHSS)" from the Research Association for steel Application (FOSTA), Düsseldorf, was supported by the Federal Ministry of Economic Affairs and Climate Action through the German Federation of Industrial Research Associations (AiF) as part of the programme for promoting industrial cooperative research (IGF) on the basis of a decision by the German Bundestag. The project was carried out at the Fraunhofer Institute for Mechanics of Materials IWM.

8 Literature

- [1] VDA238-100 (Prüfblatt)/VDA 238-100 (test specification), Dezember 2010/December 2010
- [2] Bai, Y., Wierzbicki, T: "A new model of metal plasticity and fracture with pressure and lode dependence", International Journal of Plasticity, 2008, 1071–1096
- [3] Rice, J.R., Tracey, D.M.: "On the ductile enlargement of voids in triaxial stress fields", Journal of the Mechanics and Physics of Solids 17, 1969, 201–217
- [4] Neuhauser, F.M., Terrazas, O., Manopulo, N. et al: "The bending dependency of forming limit diagrams", Int. J. Mater. Form. 12, 2019, 815–825
- [5] Costas, M., Morin, D., Hopperstad, O.S., Børvik T., Langseth M.: "A through-thickness damage regularisation scheme for shell elements subjected to severe bending and membrane deformations", Journal of the Mechanics and Physics of Solids 123, 2018, 190-206
- [6] Johnsen, J., Holmen, J.K., Gruben, G., Morin, D., Langseth M.: "Calibration and Application of GISSMO and * MAT_258 for Simulations Using Large Shell Elements", Proceedings of the 16th International LS-DYNA User Conference, Online, 2020, 10-11.